Structural bases for the involvement of phosphatidylinositol-4,5-bisphosphate in the internalization of the cell-penetrating peptide Penetratin

Leïla Bechtella, Edward Chalouhi, Paula Milán Rodríguez, Marine Cosset, Delphine Ravault, Françoise Illien, Sandrine Sagan, Ludovic Carlier, Olivier Lequin, Patrick Fuchs, et al.

Structural bases for the involvement of phosphatidylinositol-4,5-bisphosphate in the internalization of the cell-penetrating peptide Penetratin

Leïla Bechtella[1,†], Edward Chalouhi[1,‡], Paula Milán Rodríguez[1,‡], Marine Cosset[1], Delphine Ravault[1], Françoise Illien[1], Sandrine Sagan[1], Ludovic Carlier[1], Olivier Lequin[1], Patrick F. J. Fuchs[1,2], Emmanuelle Sachon[1,3], Astrid Walrant[1,*]

[1]Sorbonne Université, École normale supérieure, PSL University, CNRS, Laboratoire des Biomolécules, LBM, 75005 Paris, France

[2]Université de Paris, UFR Sciences du Vivant, 75013 Paris, France

[3]Sorbonne Université, Mass Spectrometry Sciences Sorbonne Université, MS[3]U platform, UFR 926, UFR 927, Paris, France

ABSTRACT: Cell-penetrating peptides cross cell membranes through various parallel internalization pathways. Herein, we analyze the role of the negatively charged lipid phosphatidylinositol-4,5-bisphosphate ($PI(4,5)P_2$) in the internalization of Penetratin. Contributions of both inner leaflet and outer leaflet pools of $PI(4,5)P_2$ were revealed by quantifying the internalization of Penetratin in cells treated with $PI(4,5)P_2$ binders. Studies on model systems showed that Penetratin has a strong affinity for $PI(4,5)P_2$, and interacts selectively with this lipid, even in the presence of other negatively charged lipids, as demonstrated by affinity photocrosslinking experiments. Differential scanning calorimetry experiments showed that Penetratin induces lateral segregation in $PI(4,5)P_2$-containing liposomes, which was confirmed by coarse-grained molecular dynamics simulations. NMR experiments indicated that Penetratin adopts a stabilized helical conformation in the presence of $PI(4,5)P_2$-containing membranes, with an orientation parallel to the bilayer plane, which was also confirmed by all-atom simulations. NMR and photocrosslinking experiments also suggest a rather shallow insertion of the peptide in the membrane. Put together, our findings suggest that $PI(4,5)P_2$ is a privileged interaction partner for Penetratin and that it plays an important role in Penetratin internalization.

INTRODUCTION

Cell-penetrating peptides (CPPs) are defined as short amino acid sequences able to enter cells and to deliver biologically active molecules such as nucleic acids, proteins, nanoparticles, drugs or diagnostic agents, in cells and tissues. In 1991, evidence of the translocation of the 60 amino acid Antennapedia homeodomain was reported[1]. Thereafter, the short 16 residue peptide sequence, pAntp(43–58), called Penetratin (sequence ^{43}RQIKIWFQNRRMKWKK^{58}-NH_2, helical wheel projection with residue numbering on Figure S1), was proved to be responsible of this translocation property[2]. Penetratin, together with the Tat peptide, responsible of the translocation of the HIV Tat protein[3], were the first described members of the so-called CPP family.

CPPs follow two distinct pathways for their internalization in cells: endocytosis and direct translocation. They can use these two routes concomitantly, in different proportions, depending on their nature, cell type and various environmental factors. Aside from the well-described endocytic routes, many models have been proposed to explain how CPPs could cross the plasma membrane. The variability in internalization efficiency according to the cell type and peptide sequence implies that CPPs associate with various interaction partners at the membrane surface. The negatively charged lipids and carbohydrates are considered to be the first molecular partners to be encountered by positively charged CPPs[4]. Many studies have investigated the interaction of Penetratin with negatively charged model membranes through various methods. It is now clearly admitted that Penetratin strongly interacts with anionic lipids[5–7], and that they are involved in Penetratin translocation through membranes[8–11].

$PI(4,5)P_2$ is an anionic lipid carrying 3 to 5 negative charges at physiological pH[12]. $PI(4,5)P_2$ has multiple functions such as second-messenger precursor, regulator of actin polymerization, membrane trafficking, and receptor-mediated signaling[13]. It is mostly localized in the inner leaflet of the plasma membrane, even though up to 20% of $PI(4,5)P_2$ was found in the outer leaflet of human erythrocyte membranes[14]. The presence of $PI(4,5)P_2$ in the outer leaflet of the plasma membrane was recently generalized to various human cell lines and was shown to be implicated in the regulation of cell adhesion and motility[15].

Several studies have brought the focus on the unique role of $PI(4,5)P_2$ in unconventional secretion pathways for the HIV-1 Tat Protein[16], the Fibroblast Growth Factor (FGF2) [17] and more recently the homeoprotein Engrailed-2 (En-2)[18]. $PI(4,5)P_2$ has been shown to be the target of cytotoxic membrane-active peptides such as the plant defensins NaD1[19–21], TPP3[22] and NoD173[23], human defensin HBD-2[24] or the chimeric peptide TAT-$RasGAP_{317-326}$[25]. $PI(4,5)P_2$ has also been shown to be a binding partner for cyclic CPPs and has been proposed to play a role in their uptake mechanism[26]. Interestingly, another phosphoinositide, PI(3)P, has been shown to mediate the entry

of pathogen effector proteins containing RXLR-like motifs into plant and animal cells[27].

Previous work from our group has suggested a role for $PI(4,5)P_2$ in the kinetics of Penetratin internalization[28]. Very recently, a direct involvement of $PI(4,5)P_2$ in the internalization of En-2 was demonstrated, in addition to its role in secretion[18]. This is of high significance as Penetratin is derived from a homeoprotein, Antennapedia, highly related to En-2. The cell-penetrating sequence derived from En-2 shares 81% similarity with Penetratin and has very close behavior in terms of internalization and interactions in a membrane-mimicking environment[29]. This study, however, provides no direct analysis of the interaction between En-2 and $PI(4,5)P_2$.

The present work aims to analyze the role of the negatively charged lipid $PI(4,5)P_2$ as a binding partner of the CPP Penetratin and as a potential effector of Penetratin internalization and provide structural bases to decipher its involvement, using several complementary approaches. First, the involvement of $PI(4,5)P_2$ in Penetratin uptake was quantified in CHO cells, using neomycin[30] and the Pleckstrin Homology domain of phospholipase C delta 1 ($PH\text{-}PLC^{\delta}$)[31] to block $PI(4,5)P_2$. Binding of Penetratin to $PI(4,5)P_2$, and its effect on the lateral organization of $PI(4,5)P_2$ was evaluated using differential scanning calorimetry (DSC), affinity photocrosslinking[32] and coarse-grained (CG) molecular dynamics (MD) simulations. Penetratin structure, orientation and insertion in $PI(4,5)P_2$-containing model membranes was studied by NMR and all-atom MD simulations.

RESULTS

$PI(4,5)P_2$ is implicated in Penetratin internalization, and inner leaflet and outer leaflet pools have opposite effects. In order to study the contribution of $PI(4,5)P_2$ in Penetratin uptake, we quantified the internalization of the peptide $Biot(O_2)\text{-}Gly_5$-Penetratin in wild-type Chinese Hamster Ovary cells (CHO-K1) by mass spectrometry (MS)[33], using different treatments to block binding to $PI(4,5)P_2$. For every condition, we quantified the amount of internalized peptide after 15, 30 and 60 min incubation (Figure 1).

First, we pre-treated the cells with neomycin, an aminoglycoside antibiotic that binds $PI(4,5)P_2$ with high affinity[30] (Figure 1A). Neomycin potentially blocks both inner leaflet and outer leaflet pools of $PI(4,5)P_2$, and was previously used to study the involvement of $PI(4,5)P_2$ in Penetratin internalization[28] and En-2 secretion and internalization[18]. Blocking $PI(4,5)P_2$ with neomycin diminishes the internalization of Penetratin at short incubation times (15 and 30 min) but does not significantly affect internalization at 60 min, as already reported previously[28].

To specifically study the effect of the most abundant pool of $PI(4,5)P_2$, that resides in the inner leaflet, we used cells transfected with a vector expressing the GFP-tagged $PH\text{-}PLC^{\delta}$ (GFP-PH) (Figure 1B). $PH\text{-}PLC^{\delta}$ is known to selectively interact with $PI(4,5)P_2$ and its expression in cells impairs the level of available $PI(4,5)P_2$ at the membrane inner leaflet. This strategy has previously been used to study the role of $PI(4,5)P_2$ in the mechanism of action of the defensin TPP3 for example[22]. The GFP tag allowed us to assess the transfection efficiency by flow-cytometry (64% to 82%) and to quantify the internalization in transfected cells only. Transfection with GFP-PH globally decreased the amount of internalized Penetratin, with an extremely significant effect at 60 min. This slightly differs with the results observed with neomycin, and suggests that $PI(4,5)P_2$ at the inner leaflet is involved in Penetratin uptake. This is consistent with what was observed for the internalization of En-2, where depletion of $PI(4,5)P_2$ at the inner leaflet using cells overexpressing OCRL, an inositol polyphosphate 5-phosphatase, led to the decrease of En-2 uptake[18].

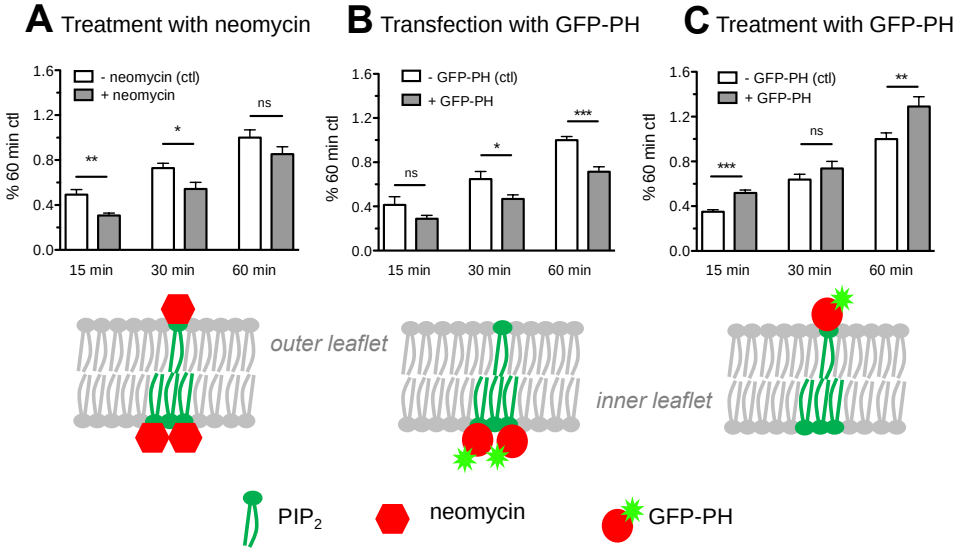

Figure 1: $PI(4,5)P_2$ is implicated in Penetratin internalization. Penetratin uptake in 10^6 CHO-K1 cells was quantified using MALDI-TOF MS, after 15 min, 30 min and 60 min of incubation with 10 µM extracellular Penetratin. 1A: cells were pre-treated with 10 mM neomycin, 30 min before incubation with Penetratin, blocking $PI(4,5)P_2$ at both membrane leaflets. 1B: cells were transfected with GFP-PH, 24h before incubation with Penetratin, blocking $PI(4,5)P_2$ at the inner leaflet. 1C: cells were pre-incubated with 0.1 µM recombinant GFP-PH 30 min before incubation with Penetratin, blocking $PI(4,5)P_2$ at the outer leaflet. Uptake in treated or transfected cells (grey bar) was compared with an untreated control (white bar). The data are normalized against the control experiment after 60 min incubation. Data are represented as average ± SEM, n≥3. Significance was tested using a Student's t-test (ns, $p>0.05$; *, $0.01<p<0.05$; **, $0.001<p<0.01$; ***, $p<0.001$)

We also tested whether the minoritarian pool of PI(4,5)P_2 located at the outer leaflet could play a role in Penetratin uptake. We thus studied the internalization of Penetratin in cells preincubated with non-permeating recombinant GFP-PH to selectively block the outer leaflet pool of PI(4,5)P_2 (Figure 1). Interestingly, treatment with extracellular GFP-PH had the opposite effect on internalization as compared to intracellularly transfected GFP-PH, *i.e.* increase of Penetratin uptake, with a very significant effect at 60 min. These results suggest that the outer leaflet pool of PI(4,5)P_2 could act as a "trap" for Penetratin, sequestering it and preventing it from crossing the membrane. A similar role has previously been proposed for sialic acids, also found at the outer leaflet of cells[34]. Its potential role in En-2 trafficking was not investigated[18].

Put together, our results suggest opposite contributions of the outer and inner leaflets pools of PI(4,5)P_2. These results are consistent with what was observed with neomycin, where blocking PI(4,5)P_2 on both leaflets leads to partly compensating responses.

To understand how PI(4,5)P_2 acts in Penetratin uptake, we then studied the interactions of Penetratin with PI(4,5)P_2 on simplified model systems, with a focus on the effect of Penetratin on the lateral organization of PI(4,5)P_2-containing membranes, Penetratin structure and insertion in the membrane and key molecular motifs involved in the interaction.

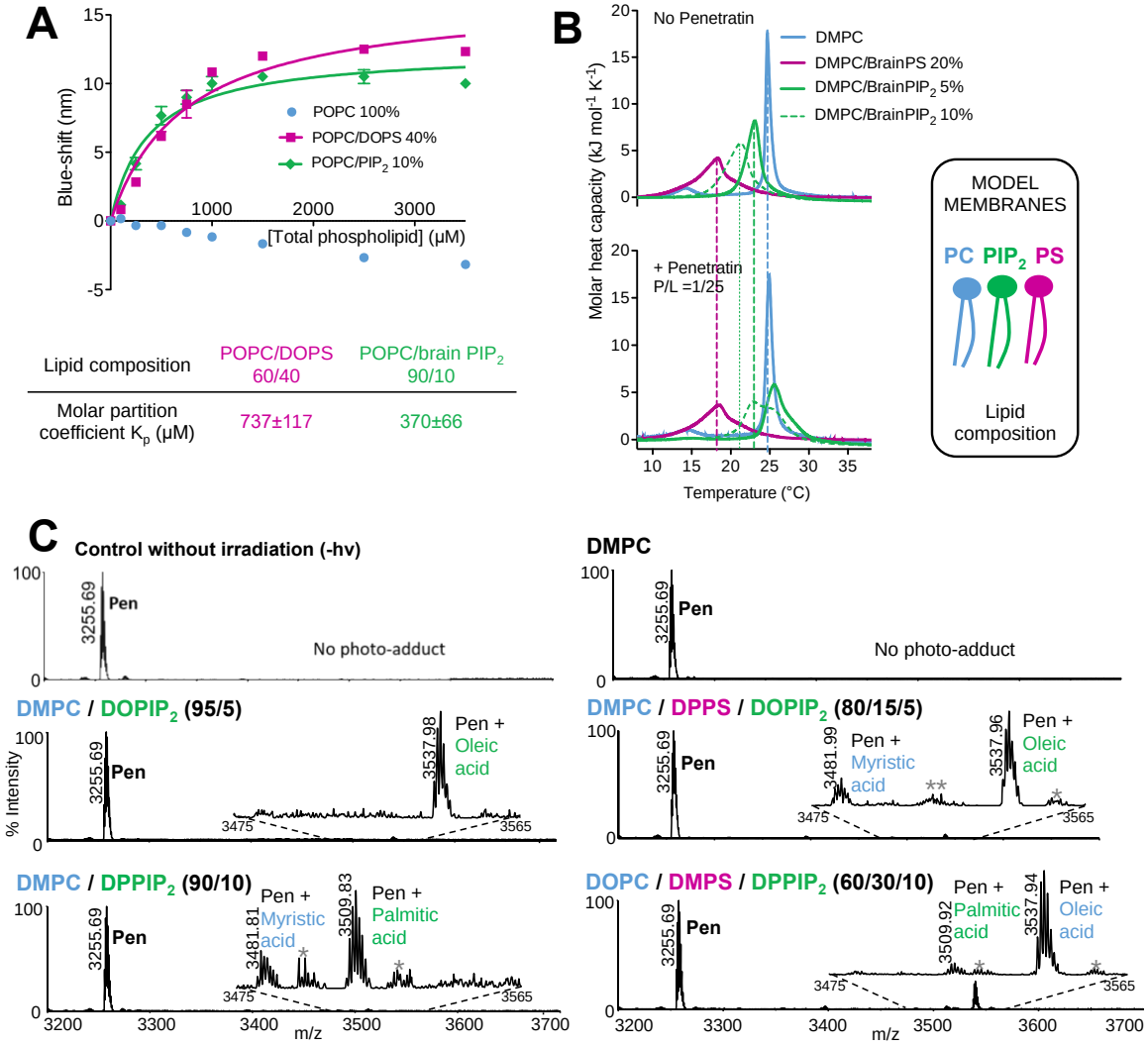

Figure 2: Penetratin interacts with PI(4,5)P_2 more favorably than with PS and recruits PI(4,5)P_2 in its immediate environment. 2A: Penetratin partitioning in POPC (blue dots), POPC/DOPS (60/40) (purple squares) and POPC/Brain PI(4,5)P_2 (90/10) (green diamonds), followed by monitoring the shift in the maximum emission wavelength of tryptophan fluorescence. Each data point is the average of three independent experiments, error bars represent SEMs. The data were fitted with a simple binding curve. The derived K_p are given in the table. 2B: DSC heating thermograms of DMPC (blue), DMPC/Brain PS (80/20) (magenta), DMPC/Brain PI(4,5)P_2 (95/5) (green solid) and DMPC/Brain PI(4,5)P_2 (90/10) (green dotted) in the absence (top) and presence (bottom) of Penetratin at a peptide-to-lipid ratio of 1/25. 2C: Representative MALDI-TOF spectra of photocrosslinking experiments with pure DMPC, binary PC/PI(4,5)P_2 and ternary PC/PS/PI(4,5)P_2 mixtures. *: +Me, +ox; **: unresolved signal which could correspond to palmitic acid, suggesting a very slight interaction with PS.

Penetratin preferentially binds and recruits PI(4,5)P_2 in its immediate surrounding, creating PI(4,5)P_2-enriched domains. In order to decipher the role of PI(4,5)P_2 as an effector of Penetratin internalization, we studied how Penetratin interacted with PI(4,5)P_2-containing model membranes as compared to PS-containing membranes. We always used four-fold more PS than PI(4,5)P_2, to take into account an average charge of –4 for PI(4,5)P_2 at physiological pH.

First, we determined molar partition coefficients of Penetratin in lipid bilayers by titrating large unilamellar vesicles (LUVs) into a solution of Penetratin and following maximum emission wavelength of intrinsic tryptophan fluorescence. When using POPC/DOPS (60/40) or POPC/brain PI(4,5)P_2 (90/10), we observed a marked blue-shift due to a change in polarity of the tryptophan environment (Figure 2A). When fitting the titration data with a simple binding curve, molar partition coefficients K_p can be determined. The K_p for PS-containing LUVs is two-fold higher than for PI(4,5)P_2, showing that Penetratin binds PI(4,5)P_2 preferably even if the global negative charge of the LUVs is identical. No blue shift, and even a slight red shift with 100% POPC LUVs, suggesting Penetratin does not insert in LUVs in the absence of negatively charged lipids.

We then studied the effect of Penetratin on the thermotropic behavior of multilamelallar vesicles (MLVs) composed of DMPC, DMPC/brain PS (80/20) or DMPC/brain PI(4,5)P_2 (95/5 and 90/10) (Figure 2B). As reported before[6], the addition of Penetratin has no effect on the phase transitions of DMPC alone. Interestingly, addition of Penetratin also had no effect on the phase transition peak of a DMPC/brain PS (80/20) mixture. On the other hand, Penetratin had a marked effect on MLVs composed of DMPC/brain PI(4,5)P_2. Addition of Penetratin leads to a shift of T_m to a higher temperature (close to that of DMPC alone) and a splitting of the transition peak, more visible with 10% PI(4,5)P_2. This suggests lateral segregation of the lipids with the formation of PI(4,5)P_2-enriched domains around Penetratin, and PI(4,5)P_2-depleted domains having a thermotropic behavior closer to that of pure DMPC.

We also studied the interactions of Penetratin with PI(4,5)P_2-containing membranes using a photocrosslinking coupled to MALDI-TOF MS approach developed in our group (Figure 2C). This strategy had previously shown that Penetratin had a preference for negatively charged lipids[35] and that in-depth spectrum analysis could yield structural information on the interaction directly at the MS level[36]. Here, we used a Penetratin derivative carrying a photactivatable benzophenone (Bzp) moiety and a biotin tag at its the *N*-terminus (Bzp-Pen). We studied the preference of Bzp-Pen for specific lipids by using MLVs of various compositions. To simplify data acquisition, we performed a saponification step before MS analysis, so that the photoadducts are only composed of the peptide crosslinked to a fatty-acid[37]. Thus, we carefully adapted the liposome compositions to match a given head-group with a given fatty-acid[35]. For all experiments, the observed photoadducts and corresponding crosslinked lipid are summarized in Table S1.

In the presence of pure DMPC liposomes, no photoadduct is observed, suggesting that Bzp-Pen does not interact with PC lipids with high affinity, consistently with the results presented above. When using a DMPC/DOPI(4,5)P_2 (95/5) mixture, a photoadduct corresponding to the crosslink of an oleic acid suggests a strong interaction between Bzp-Pen and PI(4,5)P_2. Because unsaturated fatty-acids are more reactive towards Bzp[38], we checked that no bias was introduced by using a DMPC/DPPI(4,5)P_2 (90/10) mixture. Even though Bzp-Pen has a known preference for shorter fatty acid chains[35], the most abundant photoadduct corresponds to the crosslink of a palmitic acid, thus confirming the strong preference of Bzp-Pen for PI(4,5)P_2, regardless of the nature of the fatty-acid chains. Interestingly, a photoadduct corresponding to the crosslink of a myristic acid (thus coming from DMPC) is also observed, suggesting that the presence of 5% PI(4,5)P_2 in the bilayer triggers the binding of Bzp-Pen, and that it is then capable of crosslinking any lipid in its close environment. We also studied the interaction of Penetratin with MLVs composed of DMPC/DOPS (70/30) and DMPC/DPPS (70/30) and observed the same trend (Figure S2).

We then studied whether Penetratin showed a preference towards PI(4,5)P_2 over PS by using ternary PC/PS/PI(4,5)P_2 mixtures (DMPC/DPPS/DOPI(4,5)P_2 80/15/5 or DOPC/DMPS/DPPI(4,5)P_2 60/30/10). Interestingly, we never observed PS photocrosslinking, regardless of the fatty acid chains. The observed photoadducts always corresponded to PI(4,5)P_2 and PC, probably due to its large excess compared to PS. These results confirm the marked preference of Penetratin towards PI(4,5)P_2 over PS.

In order to get molecular insights on how Penetratin leads to a lateral reorganization of PI(4,5)P_2-containing membranes, we carried out CG MD simulations. Four different systems were constructed: two Penetratin-containing systems composed of POPC/POPS/PI(4,5)P_2 (80/15/5) and POPC/POPS (80/20) as a control system, and two systems with the same membrane compositions but without Penetratin. Two snapshots of the POPC/POPS/PI(4,5)P_2/Penetratin simulation are presented in Figure 3A. They correspond to an upper view of the bilayer taken at 0 and 5416 ns of the production phase, showing the initial and final placement of the peptide relative to the lipids. All lipids were placed randomly so that there was no bias in the relative position of the lipids within the system. At 0 ns of the production phase, two PI(4,5)P_2 molecules were already located in the Penetratin surroundings. These two molecules already approached Penetratin during the equilibration phase of 10 ns, prior to the production phase. Once the production proceeded, all five PI(4,5)P_2 lipids approached Penetratin, and eventually stayed within its immediate surroundings. This phenomenon happened within the first 100 ns and the enrichment was maintained until the end of the simulation. The second snapshot shows the system at 5416 ns, where the enrichment of PI(4,5)P_2 around Penetratin is clearly observed.

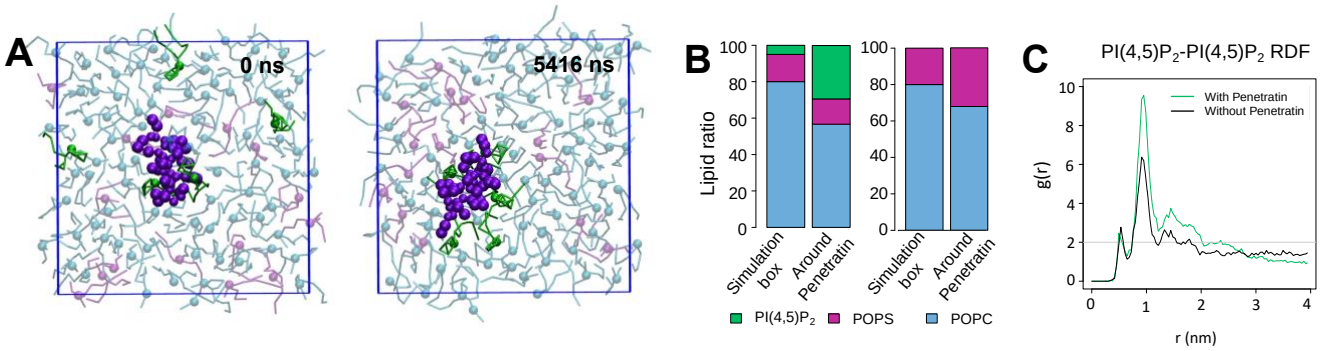

Figure 3: PI(4,5)P$_2$ clustering by Penetratin. 3A: Snapshots of the MD simulation (top view of the bilayer) taken at *t*=0 ns and *t*=5416 ns (note that all snapshots between 0.1 and 10 µs show comparable clustering). Penetratin is showed in purple balls, PC in blue, PS in magenta and PI(4,5)P$_2$ in green. 3B: Lipid ratios (PC/PS/PI(4,5)P$_2$ left, PC/PS right) at the end of the simulations, in the whole simulation box and around Penetratin (6.5 Å). 3C: Radial distribution functions of PI(4,5)P$_2$ showing the density of PI(4,5)P$_2$ as a function of distance between molecules in the presence (green) or absence (black) of Penetratin.

To have a quantitative measurement of this clustering, the ratio of each lipid type in the box at the end of the simulation is compared to its ratio around Penetratin in Figure 3B. Lipids located at a distance of 6.5 Å or smaller are considered as interacting with Penetratin. The plot on the left shows lipid ratios in POPC/POPS/PI(4,5)P$_2$/Penetratin simulation. The ratio of PI(4,5)P$_2$ around Penetratin is 5.9 times higher than the global ratio of PI(4,5)P$_2$ in the simulation box. These results are in agreement with the DSC and photocrosslinking experiments. The plot on the right shows the same analyses applied to the control POPC/POPS simulation. In the absence of PI(4,5)P$_2$, Penetratin interacts slightly more with POPS due to its negative charge, though no clear enrichment of PS in its immediate environment is observed.

It is also interesting to analyze the effect of Penetratin on PI(4,5)P$_2$ to PI(4,5)P$_2$ relative position. Intuitively, the negative charges carried by PI(4,5)P$_2$ should prevent these lipids to assemble, but this is not the case. Figure 3C shows the radial distribution function (RDF) between PI(4,5)P$_2$ molecules in the presence or absence of Penetratin. This RDF represents the probability of finding another PI(4,5)P$_2$ molecule as a function of the distance relative to a PI(4,5)P$_2$ molecule. In the absence of Penetratin, a peak around 1 nm that reaches an RDF value of around 3 can already be observed. It reflects the intrinsic tendency of PI(4,5)P$_2$ to cluster. This phenomenon has already been observed in MARTINI simulations[39] as well as experimentally on giant vesicles[40]. Interestingly, this peak at 1 nm is 1.5 times higher when Penetratin is added, meaning that PI(4,5)P$_2$ molecules will be on average closer to each other thanks to the positive charges of Penetratin. Similar simulations were performed with Penetratin in only one leaflet and PI(4,5)P$_2$ in either the same or the opposite leaflet (Figure S3). These simulations show that Penetratin and PI(4,5)P$_2$ need to be in the same leaflet to observe PI(4,5)P$_2$ clustering.

All these results show that PI(4,5)P$_2$ is a privileged interaction partner for Penetratin, and that Penetratin is able to reorganize a lipid bilayer containing low amounts of PI(4,5)P$_2$ by creating PI(4,5)P$_2$ clusters.

Penetratin adopts a stabilized helical secondary structure and inserts in model membranes containing PI(4,5)P$_2$. We investigated the effect of PI(4,5)P$_2$ on Penetratin structure by NMR, using bicelles as membrane mimetics. The ratio of long chain lipid to short chain lipid was set to 0.3 in order to get small isotropically tumbling bicelles compatible with high resolution liquid state NMR studies. Two bicelle compositions were used: zwitterionic bicelles made of 75 mM DHPC and 25 mM DMPC and anionic bicelles with the same DHPC/DMPC composition and incorporating 5% brain PI(4,5)P$_2$.

The secondary structure of Penetratin was probed at the residue level by measuring the chemical shift deviations (CSDs) of Hα protons with respect to random coil values (Figure 4A). Penetratin residues display small negative Hα CSDs in aqueous solution (average value of –0.10 ppm), indicative of a weak helical propensity in water. In the presence of zwitterionic bicelles, the CSDs become strongly negative throughout the sequence (average of –0.28 ppm), showing that Penetratin interacts with zwitterionic bicelles and adopts a stable helical structure. The CSDs become slightly more negative upon the addition of 5% PI(4,5)P$_2$ (average of –0.30 ppm), indicating that the interaction with PI(4,5)P$_2$ marginally stabilizes the helical conformation. NMR structures were calculated using ϕ and ψ dihedral angle restraints based on Hα CSDs analysis and distance restraints inferred from ^{1}H-^{1}H NOEs. Penetratin adopts a well-defined helical structure with numerous van der Waals interactions between *i*/*i*+3 and *i*/*i*+4 residues, as inferred from the observation of 30 medium-range NOEs (Figure S4).

To get information on the position of Penetratin with respect to the lipid bilayer surface, we measured paramagnetic relaxation enhancements (PREs) induced by a liposoluble paramagnetic probe, 1-palmitoyl-2-stearoyl-(5-doxyl)-sn-glycero-3-phosphocholine (5-doxyl-PC, Figure S5). The paramagnetic tag is buried inside the hydrophobic core of the membrane but its position on the C5 carbon of the acyl chain ensures a positioning close to the bilayer surface. PREs were measured by comparing the intensities of selected cross-peaks on 2D TOCSY spectra in the absence and in the presence of 5-doxyl-PC. The residual intensities are shown for each residue in Figure 4B, by selecting protons close to the backbone or protons lying further in side chains. PREs are characterized by a periodic profile that approximately matches the periodicity expected for a regular helical secondary structure. Along each successive helical turn, residues I45, F49, R53 and M54 show minimum PREs while residues I47, Q50, N51, K57, K58 have maximum values, thus delineating two faces within the helix.

This periodic profile indicates that the helix is roughly positioned parallel to the membrane surface. A small tilt in the helix orientation can be deduced from the larger residual intensities observed in the *C*-terminal part of Penetratin, suggesting that the *N*-terminus is buried deeper in the membrane whereas the *C*-terminal residues are closer to the membrane surface. Accordingly, W56 turns out to be less buried than the central W48 and F49 residues. Finally, interproton NOEs were observed between the aromatic residues of Penetratin and the lipid acyl chains, indicating that the aromatic side chains are embedded within the hydrocarbon core of the membrane.

CG MD simulations also provide information on the partitioning of the peptide within the membrane (Figure S6). We also observe the slight tilt of the α-helix, with the *N*-terminal residues more buried than the *C*-terminal ones, whether Penetratin and PI(4,5)P_2 lie in the same leaflets, or in opposite leaflet (Figure S7). Comparing the results in the presence or absence of PI(4,5)P_2 lipids, the relative position of the residues in both simulations are very similar. Since the secondary structures are maintained throughout the whole simulations, this indicates that Penetratin has a similar mean partitioning in both conditions. In contrast, we can see higher vertical fluctuations in the presence of PI(4,5)P_2, suggesting a possible influence of this lipid on the partitioning dynamics.

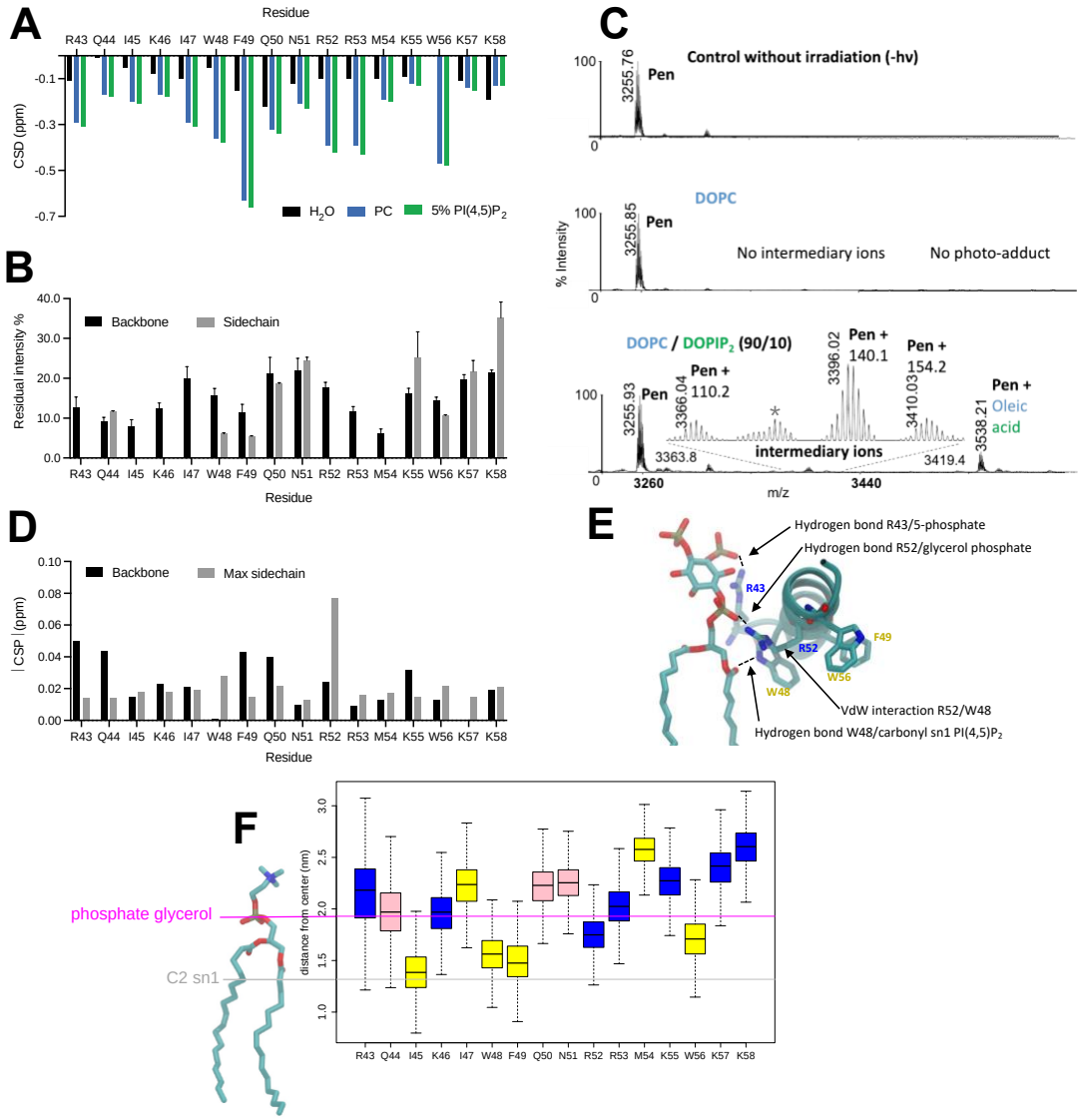

Figure 4: Structural analysis of Penetratin interaction with PI(4,5)P_2-containing membranes. 4A: NMR ^{1}Hα CSD of Penetratin residues in aqueous solution (black), zwitterionic DHPC/DMPC bicelles (blue) and bicelles containing 5% PI(4,5)P_2 (green). 4B: PREs induced by the addition of 5-doxyl PC, calculated by comparing the intensities of 2D TOCSY cross-peaks, before and after addition of the paramagnetic probe. Selected cross-peaks involve protons close to the backbone (HN-Hα and HN-Hβ correlations) or protons lying further in side chains (aromatic ring protons correlations for Phe and Trp, HN-H γ/δ correlations for Lys, side chain amide proton correlations for Asn and Gln). 4C: Representative MALDI-TOF spectra of photocrosslinking experiments with pure DOPC and binary DOPC/DOPI(4,5)P_2 showing the insertion of Penetratin in PI(4,5)P_2-containing membranes. *: +ox. 4D: CSP of backbone HN protons (black) or side chain protons (grey) induced by 5% PI(4,5)P_2 in DMPC/DHPC bicelles *vs* bicelles with no PI(4,5)P_2. In the case of side chain protons, the maximal observed CSP is reported. 4E: Selected snapshot of an all-atom MD simulation showing the interaction of Penetratin residues with a PI(4,5)P_2 lipid. 4F: Partitioning of Penetratin residues with respect to the membrane calculated on all-atom MD simulations.

Finally, photocrosslinking experiments also provided information regarding the insertion of Penetratin in membranes composed of a mixture of DOPC and DOPI(4,5)P_2 (Figure 4C). In this experimental setup, both PC and PI(4,5)P_2 lipids carry oleic acid chains, therefore, the observed oleic acid adduct cannot be attributed to either lipid, it is most probably a mixture of both. On unsaturated lipids, a fragile cyclic photoadduct can be formed by the Paternò-Büchi reaction, a [2+2] cycloaddition. Spontaneous fragmentation of this fragile photoadduct leads to the formation of fragments at m/z between Penetratin and the photoadduct, called "intermediary ions" which are informative on the position of the crosslinking on the fatty acid. [36] The process of intermediary ions formation is detailed in Figure S8. The intermediary ions are clearly visible on the mass spectrum, indicative of the presence of Bzp inserted in the close proximity of the double bond on oleic acid (C9–C10).

In order to identify the environment changes brought by PI(4,5)P_2 in NMR, we analyzed the chemical shift perturbations (CSPs) induced by the addition of 5% PI(4,5)P_2 in DHPC/DMPC bicelles (Figure 4D). These CSPs enable probing changes for each residue, which can result either from direct interaction with PI(4,5)P_2 lipids or from local conformational rearrangements. The protons that are the most sensitive to environment changes are the backbone amide protons. The chemical shift perturbations are observed all along the backbone, the NH protons of R43, Q44, F49, Q50, R52, K55 being the most affected. This suggests that residues that are implicated in PI(4,5)P_2 binding are distributed along the whole peptide sequence. On the other hand, the side chain aliphatic and aromatic protons exhibit smaller chemical shift variations, with the notable exception of R52 $CH_2\gamma$ protons. The large chemical shift variation (0.08 ppm) observed in this case may reflect a conformational rearrangement of the aromatic core of Penetratin. Indeed, the side chain protons of R52 experience a ring current shielding effect, induced by their close proximity to W48 aromatic ring (as evidenced by several W48/R52 NOEs). It is likely that the interaction of R52 with PI(4,5)P_2 leads to a reorientation of R52 side chain with respect to the aromatic moiety. It should be mentioned in this analysis that the terminal groups of Lys and Arg side chains, which are most likely to interact with PI(4,5)P_2 phosphate groups, are not visible on NMR spectra due to their fast exchange with water protons.

To get a better description of the interactions of the Penetratin residues with PI(4,5)P_2 lipids at an atomic resolution, we performed a back-mapping of the CG POPC/POPS/PI(4,5)P_2/Penetratin systems obtained after a 10 μs trajectory into a fully atomic model. Then two all-atom MD simulations were run for a duration of 100 ns. Results show that Penetratin adopts a stable helical conformation and a parallel orientation with respect to the membrane, which is similar to CG simulations (Figures 4E and S6). A slight tilt of the α-helix is also observed, with the *N*-terminal residues being more buried than the *C*-terminal ones. These results are in good agreement with NMR PRE data. Penetratin is positioned within the membrane at the level of glycerol groups (Figure 4E). The most buried residues are I45, W48 and F49, which interact with the first methylene groups of lipid acyl chains. Most Lys and Arg side chains are found at the level of lipid polar head groups. Interestingly, R52 side chain is immersed deeper in the membrane, at the level of glycerol atoms.

The analysis of distances between PI(4,5)P_2 lipids and Penetratin residues shows that hydrogen bonds and electrostatic interactions are favored between the PI(4,5)P_2 phosphate groups and Lys and Arg cationic groups (Figure S9). One PI(4,5)P_2 lipid can interact simultaneously with several residues far apart in the peptide sequence (Figure 4D). The different partitioning of Lys and Arg residues on the two faces of the peptide leads to specific interactions with PI(4,5)P_2 phosphate groups (Figures 4D and S9). Notably, most Lys and Arg residues interact with the surface exposed phosphate groups in positions 4 and 5 of PI(4,5)P_2. In contrast, R52 interacts exclusively with the more buried phosphate group in position 1 (linked to the glycerol group). The conformational space of R53 enables this residue to interact with phosphate groups of inositol at all positions.

DISCUSSION

Penetratin and its interactions with negatively charged membrane partners have been studied for more than 20 years[4]. PG is usually used as a model negatively charged lipid for such studies despite its poor biological relevance. PG-based models allowed important advances in the molecular characterization of Penetratin and its interactions with membranes. Penetratin interacts preferentially with PG over PC [6,34,35,41], it adopts an α-helical structure in the presence of PG, though an α→β transition can be observed at high charge density or peptide concentration[42]. Penetratin also tends to form peptide-rich regions at the surface of PG liposomes[6]. Finally, PG appears as a permissive lipid for direct translocation across pure lipid membranes[5,8,10,11]. As opposed to PG, PS is a biologically relevant lipid when investigating internalization mechanisms of CPPs, but it has been more scarcely used. Penetratin has a higher affinity for PS-containing membranes than just PC, and adopts an α-helical structure in its presence[43]. Regarding direct translocation, the role of PS is not clear, as it was shown to allow direct translocation[10] or not[11], depending on the experimental setup. Interactions of Penetratin with model membranes incorporating PI(4,5)P_2 have never been studied, though it was shown that direct translocation could occur in liposomes composed of PC, PI and PI-phosphates[10].

In the present study, we showed that Penetratin partitioned more favorably in PC/PI(4,5)P_2 rather than PC/PS liposomes, at a similar global negative charge. Photocrosslinking experiments showed a systematic preference for PI(4,5)P_2 over PS. This preference for PI(4,5)P_2 over PS has also been recently reported for En-2[18]. This preference could be due to a charge-density effect, the chemical nature of the moiety carrying the negative charge, and/or the presence of a positive charge on the amine of serine. Interestingly, a charge density effect has been reported as an important factor for binding when studying CPP/GAGs interactions [44–46].

NMR experiments and MD simulations gave more detailed molecular insight on the interaction between Penetratin and PI(4,5)P_2-containing membranes. In the presence of PI(4,5)P_2, Penetratin adopts a stabilized α-helical structure. The helix is oriented parallel to the lipid bilayer and is slightly tilted, leading to a more peripheral positioning of the highly cationic *C*-terminal part. It is interesting to note that a good agreement is obtained between the MD simulations in a lipid bilayer and the

experimental NMR data obtained with isotropically tumbling bicelles. Bicelles may be considered as intermediate-sized membrane mimetics between highly curved micelles and bilayer nanodiscs. Thus the bicelles used in this study have an adequate size to accommodate an amphipathic peptide of ~15 amino acids in length, without inducing topological strain [47]. The hydrophobic residues I45, W48, F49 and W56 are anchored within the membrane, but Penetratin is not deeply inserted as its backbone is positioned at the level of lipid glycerol atoms. This mode of interaction is quite similar to that observed by NMR for a Penetratin/anionic PG bicelle system[48]. A rather shallow insertion of Penetratin had previously been suggested by photocrosslinking experiments using PG model membranes[35,36]. Such shallow insertion and parallel orientation has also been reported for $(R/W)_9$, a CPP derived from Penetratin[49].

Penetratin helix is far from being perfectly amphipathic. It can be clearly seen on a helical wheel representation (Figure S1) that R52 projects its side chain on the hydrophobic face of the helix. Therefore, Penetratin immersion within the membrane leads to a positioning of R52 side chain below the membrane surface. As revealed by MD simulations, R52 is indeed the most buried cationic residue. The localization of R52 within the hydrophobic sector of Penetratin helix may explain the small depth of Penetratin insertion as the burial of a charged group in the hydrophobic interior of the membrane would be energetically unfavorable. All-atoms simulations reveal a peculiar mode of interaction of R52 with $PI(4,5)P_2$. R52 side chain interacts exclusively with the glycerol phosphate whereas the other Lys and Arg interact with the phosphate groups in positions 4 and 5 of inositol, which lie closer to the surface.

Trp plays key role in the cell uptake of homeodomain-derived peptides as well as Arg and Trp-rich CPPs. Beside its favorable partitioning properties at water/lipid interfaces, Trp may establish cation-π interactions, as proposed for Penetratin[29] and for $(R/W)_9$[50]. More recently, Trp has been involved in energetically favorable tripartite ion pair-π interactions[51]. The NMR structures reveal that R52 side chain makes van der Waals interactions with W48. The strong shielding observed for the methylenic β, γ, δ protons of R52 can be ascribed to an aromatic ring current effect and supports a favored interaction with W48 indole group. Nevertheless, the residue contact analysis in MD trajectories indicates that cation-π or ion pair-π interactions may form transiently but are not persistent over the whole simulations. Figure 4E shows that W48 indole group may also stabilize the interaction between R52 and $PI(4,5)P_2$ by donating a H-bond to the carbonyl group of lipid acyl chain.

When considering the effect of Penetratin on the organization of the membrane, DSC experiments and MD simulations show that it can modify the lateral organization of $PI(4,5)P_2$-containing membranes by recruiting $PI(4,5)P_2$ (Figure 2B and 3). Previous DSC-based studies showed that Penetratin could recruit cardiolipin and that it induced lateral partitioning in liposomes composed of DPPC and cardiolipin[52]. Cationic peptides have been found to induce multivalent $PI(4,5)P_2$ clustering in model membranes[53], but not monovalent PS, supposing that the density of charge of the $PI(4,5)P_2$ polar heads is a key factor. Recruitment of negatively charged lipids at the cell surface and CPP accumulation in these domains could be a key factor for CPP internalization. The propensity of $PI(4,5)P_2$ to form clusters in the plasma membrane has been evidenced through binding with specific proteins[54–56]. These proteins usually contain clusters of basic residues that serve as binding site to interact electrostatically with acidic lipids of the plasma membrane, and in particular with $PI(4,5)P_2$ polar head groups, recruiting several $PI(4,5)P_2$ to form clusters. Altogether, this suggests that cationic CPP sequences could be able to recruit $PI(4,5)P_2$ through electrostatic interactions and induce $PI(4,5)P_2$ clustering, or amplify its natural tendency to cluster on its own[40].

Our internalization experiments suggest that the extracellular and intracellular pools of $PI(4,5)P_2$ play opposite roles (Figure 1). We summarized our different hypotheses to explain the possible roles of $PI(4,5)P_2$ on Figure 5.

The majority of $PI(4,5)P_2$ is present at the cytosolic leaflet of the membrane and several molecular mechanisms can be envisaged to explain the involvement of $PI(4,5)P_2$ in Penetratin internalization. Penetratin-driven $PI(4,5)P_2$ clustering could act as an "electrostatic trap" inside cells. A similar role has recently been suggested for GAGs in the unconventional, $PI(4,5)P_2$-dependent FGF2 secretion pathways, with GAGs playing the role of the "electrostatic trap" outside cells[17]. This could be seen as a mirror system to Penetratin internalization, as GAGs are known as major effectors of Penetratin internalization [28,46,57]. Another explanation that could be considered is the appearance of membrane defects at the border of $PI(4,5)P_2$/Penetratin-rich domains. These domains could have a different fluidity, as suggested by DSC, and borders of such domains are seen as regions of enhanced membrane permeability[58] and have been proposed as entry routes for CPPs[57,59]. The pool of $PI(4,5)P_2$ at the outer leaflet is minoritarian, and its biological role is still unclear. An interesting point to keep in mind is that CPPs can redistribute lipids across leaflets, as was demonstrated for Tat and PS[60]. It would be interesting to study whether Penetratin internalization leads to exposure of $PI(4,5)P_2$ at the outer leaflet thus forming a feedback loop.

Possible role of $PI(4,5)P_2$ in the internalization of Penetratin can also be considered from a cellular function point of view. $PI(4,5)P_2$ is a major player in the modulation of the actin cytoskeleton organization and endocytosis[61]. Several studies strongly suggest that the actin cytoskeleton is important for CPPs internalization[62–64]. Additionally, several CPPs have been reported to have a remodeling effect on the actin cytoskeleton network[65,66]. On the other hand, a recent study demonstrated that CPPs and homeodomains entered cells through unconventional endocytosis pathways and that drugs interfering with the actin cytoskeleton seemed to have no effect of the uptake of the chimeric CPP TAT-$RasGAP_{317–326}$[67]. Again, in that perspective, the biological role of $PI(4,5)P_2$ in the internalization of Penetratin remains to be clarified. The effect of $PI(4,5)P_2$ sequestering by PH-PLC^{δ} or neomycin on internalization of Penetratin could be a combination of direct and undirect effects.

In conclusion, our study clearly identifies $PI(4,5)P_2$ as a major interacting partner for Penetratin and suggests it plays an important role for Penetratin internalization. We showed that Penetratin can drive the formation of $PI(4,5)P_2$ clusters and provided a detailed structural description of its interaction with $PI(4,5)P_2$-containing membranes. Exactly how $PI(4,5)P_2$ contributes to Penetratin internalization remains to be determined by a finer mechanistic analysis of the processes involved in $PI(4,5)P_2$-dependent uptake.

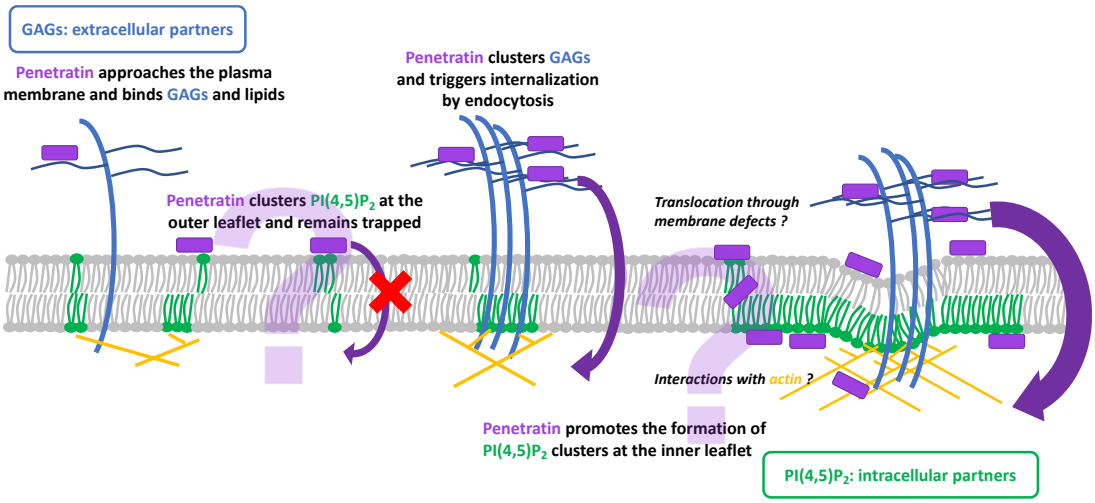

Figure 5: Cartoon model illustrating the possible contributions of PI(4,5)P2 in Penetratin internalization.

METHODS

More detailed methods are given in supporting information.

Peptide synthesis and protein production. Different Penetratin analogues were used according to the experiment. Pen corresponds to the amino acid sequence RQIKIWFQNRRMKWKK. Ac-Pen-NH_2, used in NMR experiments, was obtained from the Peptide Synthesis Platform, IBPS, Sorbonne Université. Biot(O_2)-G_5-Pen-NH_2 and Biot(O_2)-G(2,2-^2H)$_5$-Pen-NH_2, used in internalization experiments, Biot(O_2)-Apa-Pen-NH_2 used in DSC and fluorescence experiments, Biot(O_2)-Apa-G_5-K(εBzp)-RQIKIWFQNRRM(O_2)KWKK-NH_2 used in photo-crosslinking experiments were synthesized manually using Boc solid-phase peptide synthesis and purified by RP-HPLC.

GST-PH-PLC$^{\delta}$-GFP was recombinantly expressed in *E. coli* BL21 and purified using Glutathione Sepharose 4B beads (GE Healthcare), according to the supplier's instructions. The plasmids pGEX 4T2 PH-PLC$^{\delta}$-GFP and pCS2 GFP-PH-PLC$^{\delta}$ were a kind gift from Jennifer Gallop (Gurdon Institute and Biochemistry Department, Cambridge University, UK).

Internalization quantification and transfection with GFP-PH-PLC$^{\delta}$. Quantification of Penetratin internalization by MALDI-TOF MS was performed as described previously[33].

For experiments with neomycin treatment, cells were preincubated for 30 min with 10 mM of neomycin sulfate (Sigma Aldrich) prior to peptide incubation.

For experiments with GFP-PH treatment, cells were preincubated for 30 min with 0.1 µM recombinant GST-PH-PLC$^{\delta}$-GFP prior to peptide incubation.

For experiments with GFP-PH transfection, 10^5 cells were plated in 12-well culture plate 48 h before the experiment. After 24 h culture, cells were transfected with the plasmid pCS2 GFP-PH-PLC$^{\delta}$. The percentage of transfected cells was determined by flow cytometry using a FACSCalibur (BD) flow cytometer. A control experiment was performed in parallel, with cells treated with the same conditions but without DNA in the transfection step.

To compare the absolute amount of internalized Penetratin in transfected cells and control cells, we applied a correction to take the percentage of transfected cells into account. The applied correction corresponds to:

$$n(Pen_{GFP-PH}) = \frac{n(Pen_{tot}) - (1 - \alpha_{GFP-PH}) \times n(Pen_{control})}{\alpha_{GFP-PH}}$$

where n(Pen_{GFP-PH}) corresponds to the amount of Penetratin internalized in transfected cells, n(Pen_{tot}) the amount of Penetratin internalized in all the cells of the well (transfected and non-transfected), n($Pen_{control}$) the amount of Penetratin internalized in the non-transfected cells of the control experiment and α_{GFP-PH} the fraction of transfected cells.

Liposomes preparation. MLVs used in DSC and photo-crosslinking experiments, were prepared according to the standard hydrated film method in PBS pH 7.4. LUVs used in fluorescence experiments, were prepared from MLVs suspensions by extrusion through a 100 nm polycarbonate membrane.

Binding to LUVs evaluated by intrinsic Trp fluorescence. A Penetratin solution at 20 µM in PBS was titrated by adding LUVs at increasing concentration, from 0 to 3.5 mM. Trp-fluorescence spectra were acquired using a FP 8300 Jasco fluorimeter. Emission spectra were recorded from 300 to 500 nm using a 280 nm excitation wavelength. Curve fitting was performed using a simple hyperbolic saturation equation with the software GraphPad Prism.

Differential Scanning Calorimetry. DSC experiments were performed on a Nano DSC microcalorimeter (TA instruments), using MLVs at 1 mg.mL^{-1} total lipid concentration. Series of DSC heating and cooling scans were acquired using a scan rate of 1° C.min^{-1}. Data analysis was performed with the software Nano Analyze provided by TA instruments.

Photocrosslinking and MALDI-TOF MS analysis. Photocrosslinking experiments were performed on samples containing 10 nmol peptide and 100 nmol lipid (MLVs) in PBS, 200 µL total volume, as previously described[36]. After irradiation, samples were hydrolyzed by adding 200 µL of 4 M NaOH in MeOH. MALDI-TOF MS spectra were acquired on a

Voyager DEPro, a 4700 Proteomics Analyzer (Sciex) or on an Autoflex 4 (Bruker), in positive ions reflector mode using 2,5-dihydroxybenzoic acid as MALDI matrix. The m/z difference between the peptide-lipid photoadduct and the unreacted peptide indicated the nature of the lipid partner.

CG MD simulations. CG MD simulations were carried out using the MARTINI force field for lipids[68] and proteins[69] (version 2). Four different systems were constructed using the CHARMM-GUI webserver [70,71]: two Penetratin containing systems with lipid compositions POPC/POPS/PI(4,5)P_2 (80/15/5) and POPC/POPS (80/20), and two with the same membrane composition without Penetratin as control systems. Each system had 200 lipids (100 per leaflet) and 13-14 water beads per lipid. Sodium and chloride beads were added to get the system neutral and reach a salt concentration of 150 mM. Production simulations were run for 10 µs for each system. All simulations were carried out using GROMACS 2018.5[72].

All-atom MD simulations. All-atom MD simulations were performed with GROMACS 2018.5 [72] using the CHARMM36 force field [73] for lipids and CHARMM36m [74] for Penetratin. For constructing the system, we took the final frame (at 10 µs) of the first trajectory of our CG MD simulations. This CG system was back-mapped to all-atom using the CHARMM-GUI webserver [70,71]. The all-atom system is thus identical to the CG one in terms of composition. Two trajectories of 100 ns with different starting velocities were then performed in the NPT ensemble.

NMR. NMR samples were prepared in 5 mm Shigemi tubes using a volume of 300 µL. Samples contained 1 mM Ac-Penetratin-NH_2 in 50 mM sodium phosphate buffer, pH 6.05, 100 mM NaCl, 0.02% (w/v) NaN_3, 0.11 mM sodium 2,2-dimethyl-2-silapentane-5-sulfonate-d_6, in 90/10 (v/v) H_2O/D_2O. Bicelles samples contained 75 mM DHPC, 25 mM DMPC, 0 to 1.25 mM brain PI(4,5)P_2. 2D ^{1}H-^{1}H TOCSY and 2D ^{1}H-^{1}H NOESY experiments were recorded at 40°C on a Bruker Avance III 500 MHz spectrometer equipped with a TCI cryoprobe. Band-selective pulses were applied to selectively observe the amide/aromatic region in the acquisition dimension, as described previously[75]. NMR data were processed with TopSpin 3.6 program and analyzed with NMRFAM-SPARKY. PREs were monitored by quantifying cross-peaks intensities in 2D TOCSY experiments recorded in the absence or presence of 0.5 mM 5-doxyl-PC. Structures were calculated with XPLOR-NIH program using 32 φ and ψ dihedral angle restraints and 113 distance restraints. Distance to plane restraints were added in the protocol to include the positional information deduced from PRE experiments [76].

ASSOCIATED CONTENT

Supporting Information

Supporting information include more detailed experimental methods, and additional figures and tables providing more details on the structural characterization of Penetratin, additional information on photocrosslinking experiments and adduct formation mechanisms, and molecular dynamics simulations performed with Penetrain in only one leaflet.

AUTHOR INFORMATION

Corresponding Author

* Astrid Walrant, astrid.walrant@sorbonne-universite.fr

Present Addresses

† Leïla Bechtella: Institute of Chemistry and Biochemistry, Freie Universität Berlin, Arnimallee 22, 14195 Berlin, Germany.

Author Contributions

‡These authors contributed equally.
The manuscript was written through contributions of all authors. / All authors have given approval to the final version of the manuscript.

Funding Sources

LB, EC, PMR and MC were supported by a Ph.D. grant from the French Ministère de l'Enseignement Supérieur, de la Recherche et de l'Innovation (M.E.S.R.I.).
This work was supported by the Agence Nationale de la Recherche (ANR CROSS).

ACKNOWLEDGMENT

We thank the mass spectrometry MS3U Platform, Sorbonne Université for equipment and assistance. All-atom MD simulations were performed using HPC resources from GENCI-CINES allocated to P.F.J.F. from the A10 call.
We thank J. Gallop for the kind gift of the GFP-PH-PLC$^\delta$ plasmids.

ABBREVIATIONS

5-doxyl PC: 1-palmitoyl-2-stearoyl-(5-doxyl)-sn-glycero-3-phosphocholine; Bzp: Benzophenone; CG: Coarse-grained; CHO: Chinese Hamster Ovary; CPP: cell-penetrating peptide; CSD: Chemical Shift Deviation; CSP: Chemical Shift Perturbation; DHPC: 1,2-dihexanoyl-sn-glycero-3-phosphocholine; DMPC: 1,2-dimyristoyl-sn-glycero-3-phosphocholine; DMPS: 1,2-dimyristoyl-sn-glycero-3-phospho-L-serine; DOPC: 1,2-dioleoyl-sn-glycero-3-phosphocholine; DOPI(4,5)P_2: 1,2-dioleoyl-sn-glycero-3-phospho-(1'-myo-inositol-4',5'-bisphosphate); DOPS: 1,2-dioleoyl-sn-glycero-3-phosphoserine; DPPI(4,5)P2: 1,2-dipalmitoyl-sn-glycero-3-phospho-(1'-myo-inositol-4',5'-bisphosphate); DPPS: 1,2-dipalmitoyl-sn-glycero-3-phospho-L-serine; DSC: Differential Scanning Calorimetry; En-2: Engrailed-2; GAG: Glycosaminoglycan; GFP: Green Fluorescent Protein; GST: Glutathione S-transferase; LUV: Large Unilamellar Vesicle; MALDI-TOF: Matrix Assisted Laser Desorption/Ionization–Time-of-flight; MD: Molecular Dynamics; MLV: Multilamellar vesicle; MS: Mass Spectrometry; PH-PLC$^\delta$: Pleckstrin Homology Domain of Phospholipase C delta 1; PG: phosphatidylglycerol; PI(4,5)P_2: Phosphatidylinositol 4,5-bisphosphate; POPC: 1-palmitoyl-2-oleoyl-glycero-3-phosphocholine; POPS: 1-palmitoyl-2-oleoyl-sn-glycero-3-phospho-L-serine; PRE: Paramagnetic Relaxation Enhancement; RDF: Radial Distribution Function.

REFERENCES

(1) Joliot, A., Pernelle, C., Deagostini-Bazin, H., and Prochiantz, A. (1991) Antennapedia homeobox peptide regulates neural morphogenesis. *Proc. Natl. Acad. Sci. 88*, 1864–1868.
(2) Derossi, D., Joliot, A. H., Chassaing, G., and Prochiantz, A. (1994) The third helix of the Antennapedia homeodomain translocates through biological membranes. *J. Biol. Chem. 269*, 10444–10450.
(3) Vivès, E., Brodin, P., and Lebleu, B. (1997) A truncated HIV-1 Tat protein basic domain rapidly translocates through the plasma membrane and accumulates in the cell nucleus. *J. Biol. Chem. 272*, 16010–16017.
(4) Walrant, A., Cardon, S., Burlina, F., and Sagan, S. (2017) Membrane Crossing and Membranotropic Activity of Cell-Penetrating Peptides: Dangerous Liaisons? *Acc. Chem. Res. 50*, 2968–2975.
(5) Binder, H., and Lindblom, G. (2003) Charge-dependent translocation of the Trojan peptide penetratin across lipid membranes. *Biophys. J. 85*, 982–995.
(6) Alves, I. D., Goasdoué, N., Correia, I., Aubry, S., Galanth, C., Sagan, S., Lavielle, S., and Chassaing, G. (2008) Membrane interaction and perturbation mechanisms induced by two cationic cell penetrating peptides with distinct charge distribution. *Biochim. Biophys. Acta - Gen. Subj. 1780*,

948–959.
(7) Ziegler, A. (2008) Thermodynamic studies and binding mechanisms of cell-penetrating peptides with lipids and glycosaminoglycans. *Adv. Drug Deliv. Rev. 60*, 580–597.
(8) Swiecicki, J. M., Bartsch, A., Tailhades, J., Di Pisa, M., Heller, B., Chassaing, G., Mansuy, C., Burlina, F., and Lavielle, S. (2014) The Efficacies of cell-penetrating peptides in accumulating in large unilamellar vesicles depend on their ability to form inverted micelles. *ChemBioChem 15*, 884–891.
(9) Thorén, P. E. G., Persson, D., Karlsson, M., and Nordén, B. (2000) The Antennapedia peptide penetratin translocates across lipid bilayers - The first direct observation. *FEBS Lett. 482*, 265–268.
(10) Terrone, D., Sang, S. L. W., Roudaia, L., and Silvius, J. R. (2003) Penetratin and Related Cell-Penetrating Cationic Peptides Can Translocate Across Lipid Bilayers in the Presence of a Transbilayer Potential. *Biochemistry 42*, 13787–13799.
(11) Gehan, P., Kulifaj, S., Soule, P., Bodin, J. B., Amoura, M., Walrant, A., Sagan, S., Thiam, A. R., Ngo, K., Vivier, V., Cribier, S., and Rodriguez, N. (2020) Penetratin translocation mechanism through asymmetric droplet interface bilayers. *Biochim. Biophys. Acta - Biomembr. 1862*, 183415.
(12) McLaughlin, S., Wang, J., Gambhir, A., and Murray, D. (2002) PIP2 and proteins: Interactions, organization, and information flow. *Annu. Rev. Biophys. Biomol. Struct. 31*, 151–175.
(13) Katan, M., and Cockcroft, S. (2020) Phosphatidylinositol(4,5)bisphosphate: diverse functions at the plasma membrane. *Essays Biochem. 64*, 513–531.
(14) Bütikofer, P., Lin, Z. W., Chiu, D. T.-Y., Lubin, B., and Kuyperss, F. A. (1990) Transbilayer Distribution and Mobility of Phosphatidylinositol in Human Red Blood Cells. *J. Biol. Chem. 265*, 16035–16038.
(15) Yoneda, A., Kanemaru, K., Matsubara, A., Takai, E., Shimozawa, M., Satow, R., Yamaguchi, H., Nakamura, Y., and Fukami, K. (2020) Phosphatidylinositol 4,5-bisphosphate is localized in the plasma membrane outer leaflet and regulates cell adhesion and motility. *Biochem. Biophys. Res. Commun. 527*, 1050–1056.
(16) Rayne, F., Debaisieux, S., Yezid, H., Lin, Y. L., Mettling, C., Konate, K., Chazal, N., Arold, S. T., Pugnière, M., Sanchez, F., Bonhoure, A., Briant, L., Loret, E., Roy, C., and Beaumelle, B. (2010) Phosphatidylinositol-(4,5)-bisphosphate enables efficient secretion of HIV-1 Tat by infected T-cells. *EMBO J. 29*, 1348–1362.
(17) Steringer, J. P., Lange, S., Čujová, S., Šachl, R., Poojari, C., Lolicato, F., Beutel, O., Müller, H. M., Unger, S., Coskun, Ü., Honigmann, A., Vattulainen, I., Hof, M., Freund, C., and Nickel, W. (2017) Key steps in unconventional secretion of fibroblast growth factor 2 reconstituted with purified components. *Elife 6*, 1–36.
(18) Amblard, I., Dupont, E., Alves, I., Miralves, J., Queguiner, I., and Joliot, A. (2020) Bidirectional transfer of homeoprotein EN2 across the plasma membrane requires PIP2. *J. Cell Sci. 133*.
(19) Poon, I. K. H., Baxter, A. A., Lay, F. T., Mills, G. D., Adda, C. G., Payne, J. A. E., Phan, T. K., Ryan, G. F., White, J. A., Veneer, P. K., van der Weerden, N. L., Anderson, M. A., Kvansakul, M., and Hulett, M. D. (2014) Phosphoinositide-mediated oligomerization of a defensin induces cell lysis. *Elife 2014*, 1–27.
(20) Payne, J. A. E., Bleackley, M. R., Lee, T. H., Shafee, T. M. A., Poon, I. K. H., Hulett, M. D., Aguilar, M. I., Van Der Weerden, N. L., and Anderson, M. A. (2016) The plant defensin NaD1 introduces membrane disorder through a specific interaction with the lipid, phosphatidylinositol 4,5 bisphosphate. *Biochim. Biophys. Acta - Biomembr. 1858*, 1099–1109.
(21) Baxter, A. A., Poon, I. K. H., and Hulett, M. D. (2017) The plant defensin NaD1 induces tumor cell death via a non-apoptotic, membranolytic process. *Cell Death Discov. 3*, 1–11.
(22) Baxter, A. A., Richter, V., Lay, F. T., Poon, I. K. H., Adda, C. G., Veneer, P. K., Phan, T. K., Bleackley, M. R., Anderson, M. A., Kvansakul, M., and Hulett, M. D. (2015) The Tomato Defensin TPP3 Binds Phosphatidylinositol (4,5)-Bisphosphate via a Conserved Dimeric Cationic Grip Conformation To Mediate Cell Lysis. *Mol. Cell. Biol. 35*, 1964–1978.
(23) Lay, F. T., Ryan, G. F., Caria, S., Phan, T. K., Veneer, P. K., White, J. A., Kvansakul, M., and Hulett, M. D. (2019) Structural and functional characterization of the membrane-permeabilizing activity of Nicotiana occidentalis defensin NoD173 and protein engineering to enhance oncolysis. *FASEB J. 33*, 6470–6482.
(24) Järvå, M., Phan, T. K., Lay, F. T., Caria, S., Kvansakul, M., and Hulett, M. D. (2018) Human -defensin 2 kills Candida albicans through phosphatidylinositol 4,5-bisphosphate–mediated membrane permeabilization. *Sci. Adv. 4*, 1–10.
(25) Serulla, M., Ichim, G., Stojceski, F., Grasso, G., Afonin, S., Heulot, M., Schober, T., Roth, R., Godefroy, C., Milhiet, P. E., Das, K., García-Sáez, A. J., Danani, A., and Widmann, C. (2020) TAT-RasGAP317-326 kills cells by targeting inner-leaflet-enriched phospholipids. *Proc. Natl. Acad. Sci. U. S. A. 117*, 31871–31881.
(26) Cascales, L., Henriques, S. T., Kerr, M. C., Huang, Y. H., Sweet, M. J., Daly, N. L., and Craik, D. J. (2011) Identification and characterization of a new family of cell-penetrating peptides: Cyclic cell-penetrating peptides. *J. Biol. Chem. 286*, 36932–36943.
(27) Kale, S. D., Gu, B., Capelluto, D. G. S., Dou, D., Feldman, E., Rumore, A., Arredondo, F. D., Hanlon, R., Fudal, I., Rouxel, T., Lawrence, C. B., Shan, W., and Tyler, B. M. (2010) External Lipid PI3P Mediates Entry of Eukaryotic Pathogen Effectors into Plant and Animal Host Cells. *Cell 142*, 284–295.
(28) Jiao, C. Y., Delaroche, D., Burlina, F., Alves, I. D., Chassaing, G., and Sagan, S. (2009) Translocation and endocytosis for cell-penetrating peptide internalization. *J. Biol. Chem. 284*, 33957–33965.
(29) Balayssac, S., Burlina, F., Convert, O., Bolbach, G., Chassaing, G., and Lequin, O. (2006) Comparison of penetratin and other homeodomain-derived cell-penetrating peptides: Interaction in a membrane-mimicking environment and cellular uptake efficiency. *Biochemistry 45*, 1408–1420.
(30) Gabev, E., Kasianowicz, J., Abbott, T., and McLaughlin, S. (1989) Binding of neomycin to phosphatidylinositol 4,5-biphosphate (PIP2). *BBA - Biomembr. 979*, 105–112.
(31) Garcia, P., Gupta, R., Shah, S., Morris, A. J., Rudge, S. A., Scarlata, S., Petrova, V., McLaughlin, S., and Rebecchi, M. J. (1995) The Pleckstrin Homology Domain of Phospholipase C-δ1 Binds with High Affinity to Phosphatidylinositol 4,5-Bisphosphate in Bilayer Membranes. *Biochemistry 34*, 16228–16234.
(32) Walrant, A., and Sachon, E. (2021) Photolabeling Strategies to Study Membranotropic Peptides Interacting with Lipids and Proteins in Membranes. *Bioconjug. Chem. 32*, 1503–1514.
(33) Burlina, F., Sagan, S., Bolbach, G., and Chassaing, G. (2006) A direct approach to quantification of the cellular uptake of cell-penetrating peptides using MALDI-TOF mass spectrometry. *Nat. Protoc. 1*, 200–205.
(34) Alves, I. D., Bechara, C., Walrant, A., Zaltsman, Y., Jiao, C. Y., and Sagan, S. (2011) Relationships between membrane binding, affinity and cell internalization efficacy of a cell-penetrating peptide: Penetratin as a case study. *PLoS One 6*, e24096.
(35) Jiao, C. Y., Sachon, E., Alves, I. D., Chassaing, G., Bolbach, G., and Sagan, S. (2017) Exploiting Benzophenone Photoreactivity To Probe the Phospholipid Environment and Insertion Depth of the Cell-Penetrating Peptide Penetratin in Model Membranes. *Angew. Chemie - Int. Ed. 56*, 8226–8230.
(36) Bechtella, L., Kirschbaum, C., Cosset, M., Clodic, G., Matheron, L., Bolbach, G., Sagan, S., Walrant, A., and Sachon, E. (2019) Benzophenone Photoreactivity in a Lipid Bilayer to Probe Peptide/Membrane Interactions: Simple System, Complex Information. *Anal. Chem. 91*, 9102–9110.
(37) Jiao, C. Y., Alves, I. D., Point, V., Lavielle, S., Sagan, S., and Chassaing, G. (2010) Comparing lipid photo-cross-linking efficacy of penetratin analogues bearing three different photoprobes: Dithienyl ketone, benzophenone, and trifluoromethylaryldiazirine. *Bioconjug. Chem. 21*, 352–359.
(38) Markovic, D. Z., and Patterson, L. K. (1989) Radical Processes in Lipids. Selectivity of Hydrogen Abstraction From Lipids By Benzophenone Triplet. *Photochem. Photobiol. 49*, 531–535.
(39) Ingólfsson, H. I., Melo, M. N., Van Eerden, F. J., Arnarez, C., Lopez, C. A., Wassenaar, T. A., Periole, X., De Vries, A. H., Tieleman, D. P., and Marrink, S. J. (2014) Lipid organization of the plasma membrane. *J. Am. Chem. Soc. 136*, 14554–14559.
(40) Salvemini, I. L., Gau, D. M., Reid, J., Bagatolli, L. A., Macmillan, A., and Moens, P. D. J. (2014) Low PIP2 molar fractions induce nanometer size clustering in giant unilamellar vesicles. *Chem. Phys. Lipids 177*, 51–63.
(41) Binder, H., and Lindblom, G. (2003) Interaction of the Trojan peptide penetratin with anionic lipid membranes - A calorimetric study. *Phys. Chem. Chem. Phys. 5*, 5108–5117.
(42) Magzoub, M., Eriksson, L. E. G., and Gräslund, A. (2002) Conformational states of the cell-penetrating peptide penetratin when interacting with phospholipid vesicles: Effects of surface charge and peptide concentration. *Biochim. Biophys. Acta - Biomembr. 1563*, 53–63.
(43) Christiaens, B., Symoens, S., Vanderheyden, S., Engelborghs, Y., Joliot, A., Prochiantz, A., Vandekerckhove, J., Rosseneu, M., and Vanloo, B. (2002) Tryptophan fluorescence study of the interaction of penetratin peptides with model membranes. *Eur. J. Biochem. 269*, 2918–2926.
(44) Ziegler, A., and Seelig, J. (2008) Binding and clustering of glycosaminoglycans: a common property of mono- and multivalent cell-

penetrating compounds. *Biophys. J. 94*, 2142–2149.
(45) Prevette, L. E., Benish, N. C., Schoenecker, A. R., and Braden, K. J. (2015) Cell-penetrating compounds preferentially bind glycosaminoglycans over plasma membrane lipids in a charge density- and stereochemistry-dependent manner. *Biophys. Chem. 207*, 40–50.
(46) Bechara, C., Pallerla, M., Zaltsman, Y., Burlina, F., Alves, I. D., Lequin, O., and Sagan, S. (2013) Tryptophan within basic peptide sequences triggers glycosaminoglycan- dependent endocytosis. *FASEB J. 27*, 738–749.
(47) Chou, J. J., Kaufman, J. D., Stahl, S. J., Wingfield, P. T., and Bax, A. (2002) Micelle-induced curvature in a water-insoluble HIV-1 Env peptide revealed by NMR dipolar coupling measurement in stretched polyacrylamide gel. *J. Am. Chem. Soc. 124*, 2450–2451.
(48) Lindberg, M., Biverståhl, H., Gräslund, A., and Mäler, L. (2003) Structure and positioning comparison of two variants of penetratin in two different membrane mimicking systems by NMR. *Eur. J. Biochem. 270*, 3055–3063.
(49) Walrant, A., Vogel, A., Correia, I., Lequin, O., Olausson, B. E. S., Desbat, B., Sagan, S., and Alves, I. D. (2012) Membrane interactions of two arginine-rich peptides with different cell internalization capacities. *Biochim. Biophys. Acta - Biomembr. 1818*, 1755–1763.
(50) Walrant, A., Correia, I., Jiao, C. Y., Lequin, O., Bent, E. H., Goasdoué, N., Lacombe, C., Chassaing, G., Sagan, S., and Alves, I. D. (2011) Different membrane behaviour and cellular uptake of three basic arginine-rich peptides. *Biochim. Biophys. Acta - Biomembr. 1808*, 382–393.
(51) Walrant, A., Bauzá, A., Girardet, C., Alves, I. D., Lecomte, S., Illien, F., Cardon, S., Chaianantakul, N., Pallerla, M., Burlina, F., Frontera, A., and Sagan, S. (2020) Ionpair-π interactions favor cell penetration of arginine/tryptophan-rich cell-penetrating peptides. *Biochim. Biophys. Acta - Biomembr. 1862*, 183098.
(52) Joanne, P., Galanth, C., Goasdoué, N., Nicolas, P., Sagan, S., Lavielle, S., Chassaing, G., El Amri, C., and Alves, I. D. (2009) Lipid reorganization induced by membrane-active peptides probed using differential scanning calorimetry. *Biochim. Biophys. Acta - Biomembr. 1788*, 1772–1781.
(53) Golebiewska, U., Gambhir, A., Hangyás-Mihályné, G., Zaitseva, I., Rädler, J., and McLaughlin, S. (2006) Membrane-bound basic peptides sequester multivalent (PIP2), but not monovalent (PS), acidic lipids. *Biophys. J. 91*, 588–599.
(54) Gambhir, A., Hangyas-Mihalyne, G., Zaitseva, I., Cafiso, D. S., Wang, J., Murray, D., Pentyala, S. N., Smith, S. O., and McLaughlin, S. (2004) Electrostatic Sequestration of PIP2 on Phospholipid Membranes by Basic/Aromatic Regions of Proteins. *Biophys. J. 86*, 2188–2207.
(55) Charlier, L., Louet, M., Chaloin, L., Fuchs, P., Martinez, J., Muriaux, D., Favard, C., and Floquet, N. (2014) Coarse-grained simulations of the HIV-1 matrix protein anchoring: Revisiting its assembly on membrane domains. *Biophys. J. 106*, 577–585.
(56) Van Den Bogaart, G., Meyenberg, K., Risselada, H. J., Amin, H., Willig, K. I., Hubrich, B. E., Dier, M., Hell, S. W., Grubmüller, H., Diederichsen, U., and Jahn, R. (2011) Membrane protein sequestering by ionic protein-lipid interactions. *Nature 479*, 552–555.
(57) Bechara, C., Pallerla, M., Burlina, F., Illien, F., Cribier, S., and Sagan, S. (2015) Massive glycosaminoglycan-dependent entry of Trp-containing cell-penetrating peptides induced by exogenous sphingomyelinase or cholesterol depletion. *Cell. Mol. Life Sci. 72*, 809–820.
(58) Goni, F. M., and Alonso, A. (2002) Sphingomyelinases: Enzymology and membrane activity. *FEBS Lett. 531*, 38–46.
(59) Verdurmen, W. P. R., Thanos, M., Ruttekolk, I. R., Gulbins, E., and Brock, R. (2010) Cationic cell-penetrating peptides induce ceramide formation via acid sphingomyelinase: Implications for uptake. *J. Control. Release 147*, 171–179.
(60) Moore, V. D. G., and Payne, R. M. (2004) Transactivator of transcription fusion protein transduction causes membrane inversion. *J. Biol. Chem. 279*, 32541–32544.
(61) Czech, M. P. (2000) PIP_2 and PIP_3: complex roles at the cell surface. *Cell 100*, 603–606.
(62) Nakase, I., Niwa, M., Takeuchi, T., Sonomura, K., Kawabata, N., Koike, Y., Takehashi, M., Tanaka, S., Ueda, K., Simpson, J. C., Jones, A. T., Sugiura, Y., and Futaki, S. (2004) Cellular uptake of arginine-rich peptides: Roles for macropinocytosis and actin rearrangement. *Mol. Ther. 10*, 1011–1022.
(63) Nakase, I., Tadokoro, A., Kawabata, N., Takeuchi, T., Katoh, H., Hiramoto, K., Negishi, M., Nomizu, M., Sugiura, Y., and Futaki, S. (2007) Interaction of Arginine-Rich Peptides with Membrane-Associated Proteoglycans Is Crucial for Induction of Actin Organization and Macropinocytosis †. *Biochemistry 46*, 492–501.
(64) Gerbal-Chaloin, S., Gondeau, C., Aldrian-Herrada, G., Heitz, F., Gauthier-Rouvière, C., and Divita, G. (2007) First step of the cell-penetrating peptide mechanism involves Rac1 GTPase-dependent actin-network remodelling. *Biol. Cell 99*, 223–238.
(65) Delaroche, D., Cantrelle, F. X., Subra, F., Van Heijenoort, C., Guittet, E., Jiao, C. Y., Blanchoin, L., Chassaing, G., Lavielle, S., Auclair, C., and Sagan, S. (2010) Cell-penetrating peptides with intracellular actin-remodeling activity in malignant fibroblasts. *J. Biol. Chem. 285*, 7712–7721.
(66) Clavier, S., Illien, F., Sagan, S., Bolbach, G., and Sachon, E. (2016) Proteomic comparison of the EWS-FLI1 expressing cells EF with NIH-3T3 and actin remodeling effect of (R/W)9 cell-penetrating peptide. *EuPA Open Proteomics 10*, 1–8.
(67) Trofimenko, E., Homma, Y., Fukuda, M., and Widmann, C. (2021) The endocytic pathway taken by cationic substances requires Rab14 but not Rab5 and Rab7. *Cell Rep. 37*, 109945.
(68) Marrink, S. J., Risselada, H. J., Yefimov, S., Tieleman, D. P., and De Vries, A. H. (2007) The MARTINI force field: Coarse grained model for biomolecular simulations. *J. Phys. Chem. B 111*, 7812–7824.
(69) Monticelli, L., Kandasamy, S. K., Periole, X., Larson, R. G., Tieleman, D. P., and Marrink, S. J. (2008) The MARTINI coarse-grained force field: Extension to proteins. *J. Chem. Theory Comput. 4*, 819–834.
(70) Jo, S., Kim, T., Iyer, V. G., and Im, W. (2008) CHARMM-GUI: A Web-based Graphical User Interface for CHARMM. *J. Comput. Chem. 29*, 1859–1865.
(71) Qi, Y., Ingólfsson, H. I., Cheng, X., Lee, J., Marrink, S. J., and Im, W. (2015) CHARMM-GUI Martini Maker for Coarse-Grained Simulations with the Martini Force Field. *J. Chem. Theory Comput. 11*, 4486–4494.
(72) Abraham, M. J., Murtola, T., Schulz, R., Páll, S., Smith, J. C., Hess, B., and Lindah, E. (2015) GROMACS: High performance molecular simulations through multi-level parallelism from laptops to supercomputers. *SoftwareX 1–2*, 19–25.
(73) Klauda, J. B., Venable, R. M., Freites, J. A., O'Connor, J. W., Tobias, D. J., Mondragon-Ramirez, C., Vorobyov, I., MacKerell, A. D., and Pastor, R. W. (2010) Update of the CHARMM All-Atom Additive Force Field for Lipids: Validation on Six Lipid Types. *J. Phys. Chem. B 114*, 7830–7843.
(74) Huang, J., Rauscher, S., Nawrocki, G., Ran, T., Feig, M., De Groot, B. L., Grubmüller, H., and MacKerell, A. D. (2016) CHARMM36m: An improved force field for folded and intrinsically disordered proteins. *Nat. Methods 14*, 71–73.
(75) Raja, Z., AndreA, S., Abbassi, F., Humblot, V., Lequin, O., Bouceba, T., Correia, I., Casale, S., Foulon, T., Sereno, D., Oury, B., and Ladram, A. (2017) Insight into the mechanism of action of temporin-SHa, a new broad-spectrum antiparasitic and antibacterial agent. *PLoS One 12*, 1–41.
(76) Xu, C., Gagnon, E., Call, M. E., Schnell, J. R., Schwieters, C. D., Carman, C. V., Chou, J. J., and Wucherpfennig, K. W. (2008) Regulation of T Cell Receptor Activation by Dynamic Membrane Binding of the CD3ε Cytoplasmic Tyrosine-Based Motif. *Cell 135*, 702–713.

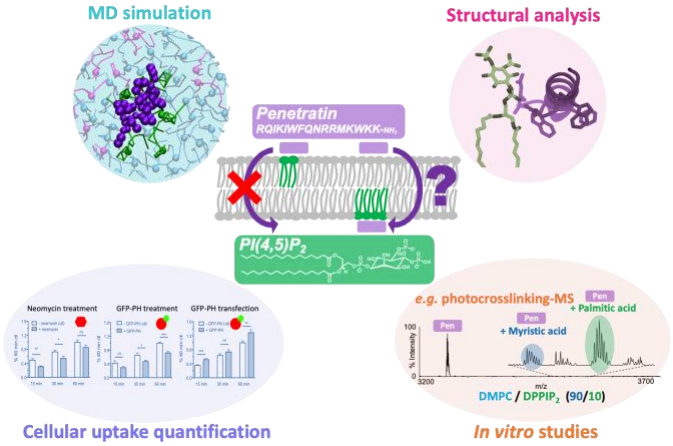
MD simulation
Structural analysis
Penetratin
RQIKIWFQNRRMKWKK-NH2
?
PI(4,5)P2
Neomycin treatment
GFP-PH treatment
GFP-PH transfection
e.g. photocrosslinking-MS
Pen
+ Palmitic acid
+ Myristic acid
% Intensity
m/z
3200
3700
DMPC / DPPIP2 (90/10)
Cellular uptake quantification
In vitro studies